



Investigation of sedimentary records of Hurricane Irma in sinkholes, Big Pine Key, Florida

Progress in Physical Geography
2021, Vol. 45(6) 885–906
© The Author(s) 2021
Article reuse guidelines:
sagepub.com/journals-permissions
DOI: 10.1177/03091333211017764
journals.sagepub.com/home/ppg



Youzhu Wang 

University of South Florida, USA

Philip Van Beynen

University of South Florida, USA

Ping Wang

University of South Florida, USA

Gregg Brooks

Eckerd College, USA

Gregory Herbert

University of South Florida, USA

Robert Tykot

University of South Florida, USA

Abstract

Few paleotempestological studies have focused on coastal sinkholes, a common feature in Florida, which can receive and preserve storm overwash sediments. The major goal of this research is to improve our understanding of the characteristic signatures of storm sediments in sinkholes thereby determining reliability of these environments as proxies for hurricanes. Hurricane Irma as a category 5 storm provides an excellent case study for characterizing storm deposits in sinkholes on Big Pine Key. We cored at four sinkholes along a 350 m transect normal to the shoreline. Core sediments were characterized using physical description, short-lived radioisotope dating, sediment grain size analysis, loss-on-ignition, microfossil analysis, and x-ray fluorescence elemental analysis. We found that Irma deposits had higher abundances of marine foraminifera, less total organic matter and elevated Si/Al and Ca/Ti ratios, compared to pre- or post-Irma sediments. In addition, there was a thinning of the storm sediments along the inland transect. Consequently, we propose that sinkholes, particularly those that are closer to the shoreline, can provide reliable sites for paleotempestology studies.

Keywords

Hurricane Irma, storm overwash, sinkholes, Florida Keys, paleotempestology, carbonate reef environment

1 Introduction

In the past 35 years, the global number of tropical cyclones identified as category 4 and 5 on the Saffir–Simpson hurricane wind scale has

Corresponding author:

Youzhu Wang, University of South Florida, 4202 E. Fowler Avenue, Tampa, FL 33620, USA.

Email: youzhu@usf.edu

doubled and the intensity of hurricanes in the Atlantic has increased with warmer sea surface temperatures (Bhatia et al., 2018; Horton et al., 2009; Patricola and Wehner, 2018; Shao et al., 2017; Snaiki et al., 2020; Webster et al., 2005). The hurricanes making landfall in the United States have led to significant losses of on average 16.7 billion USD per year for the last 118 years (1900–2017), while only in 2017 the direct economic losses were ~236 billion USD including 30 billion USD losses for Hurricane Irma (Weinkle et al., 2018). The increased activity of these tropical storms worldwide seems unprecedented, but the outputs of simulation predictions may involve many uncertainties and deviate from observed data due to the short documentary record. This creates a challenge for revealing any trend in recurrence intervals of intense hurricanes (Bregy et al., 2018; Liu et al., 2014). A reliable reconstruction of major hurricane landfalls throughout the current long-term climate interval can help estimate/determine how long-term climate changes impact on hurricane activities (Adomat and Gischler, 2017; Bilskie et al., 2016).

There are few paleotempestology records of category 4 and 5 hurricanes specifically for carbonate-specific environments. Compared to the Gulf of Mexico coast, little is known about paleotempestological sedimentary structures in the Florida Keys. Coastal sediments of the Keys differ from those of the Gulf of Mexico as the former are situated on a carbonate reef platform facing the Atlantic Ocean. The physical environment of the Keys is ideal for reef development with shallow bay water and little variability in water temperature/salinity (Vacher and Quinn, 2004). Sediments in this carbonate reef environment are mainly composed of calcium carbonate as produced in the subtidal carbonate “factory” (Chough, 2012). Storm surge from major hurricanes causes significant change to coastal morphology and damages coral reefs (Atwater et al., 2014; Weinkle et al., 2018). The entrainment of these carbonate sediments by the

intensive wave action of hurricanes creates unique overwash deposits for these reefal environments.

Since the 1990s, sediment stratigraphy, microfossils (foraminifera), and elemental changes of sediments have been the main proxies used in coastal storm studies (Hippensteel et al., 2013; Liu and Fearn, 2000; Oliva et al., 2017). Anomalous sand deposits within organic fine-grain sediments are commonly used for identifying the occurrence of hurricane landfall (Donnelly and Woodruff, 2007). Because of their high diversity, narrow environmental tolerances, and relative ease of collection, foraminifera are reliable indicators of environmental conditions, especially depth, salinity, nutrients, and bottom oxygen levels (Carnahan et al., 2009; Culver, 1990; Hallock et al., 2003; Ishman et al., 1997; Sen Gupta, 1999). Consequently, foraminiferal assemblages have been used to infer paleostorm events, which can be recognized in storm-surge overwash of the test characteristic of deeper shelf species (Hawkes and Horton, 2012; Hippensteel and Martin, 1999; Hippensteel et al., 2005; Lane et al., 2011; Pilarczyk et al., 2014; Scott et al., 2003). Abrupt changes in assemblages can show the provenance of the storm deposits, which can help determine the characteristics of storm strength and track of the storm (Horton et al., 2009; Scott et al., 2003). In addition, X-ray fluorescence (XRF) core scanning has been applied for paleotempestological research. Changes in the elemental signatures of sediments determined by XRF can be helpful to identify storm deposits even though other proxies may not (Liu et al., 2014; Oliva et al., 2018; Swindles et al., 2018; Yao et al., 2018).

This study documents sedimentary characteristics of Hurricane Irma in coastal sinkholes at Big Pine Key (BPK), Florida, using a multi-proxy approach including geochronology, grain size analysis, loss-on-ignition (LOI), foraminiferal assemblages, and XRF. We explore how the characteristics of these storm sediments change

along a transect of inland sinkholes. A 16 km offshore transect to a depth of 20 m was undertaken to sample and determine the characteristics of marine sediments that may be entrained by a major storm such as Hurricane Irma. Of particular interest is whether foraminiferal assemblage representative of different water depths can be distinguished in the sinkhole deposits, specifically whether the occurrence of deeper-water forams is characteristic of the wave energy of a category 4 hurricane. Also, we determine the environmental contributions of various sources of sediments (such as offshore, beach, surrounding soils, etc.) to the storm deposits and how well the storm deposits are preserved in the sinkholes. The results of this study could help with the future interpretation of storm deposits found in sinkholes located on carbonate platforms which are characteristic of many Caribbean Islands that experience hurricane activity. We should also note that there are few studies of hurricane sediments in the Florida Keys.

II Study area

The Florida Keys, USA, consist of tropical islands along a 240 km chain started from the southern continental shelf of Florida, westward to Gulf of Mexico and eastward to Atlantic Ocean (Vacher and Quinn, 2004). Big Pine Key (BPK, Figure 1) (24°38'11" N, 81°20'47" W), approximately 10 km in length and 3 km in width, is the biggest island of the lower Keys (Braden et al., 2005). This low-lying island has a maximum elevation of 2 m (Langevin et al., 1998).

The bedrock type of Upper Florida Keys is mainly Key Largo Limestone, and Lower Florida Keys are composed of Miami Oolitic Limestone. The contact of these two formations occurs at BPK, which is the Miami Limestone, averaging 5.7 m in thickness, and overlies the Key Largo Limestone (Hanson, 1980). The Miami oolitic layer can prevent the mixing of

freshwater and saltwater, which protects BPK groundwater from saltwater intrusion (Saha et al., 2011).

The climate of BPK is tropical with temperatures ranging from 20°C in January to 29°C in August and has 102.2 cm average annual precipitation (Ogurcak and Price, 2019). Approximately 75–85% precipitation occurs during the wet season from May to October, which includes the hurricane season.

The vegetation is diverse on BPK and is distributed according to elevation. Coastal vegetation includes mangroves and buttonwood forests. As elevation increases, vegetation transitions into pineland, hardwood, and saw palmetto (Harveson et al., 2004). Florida Key deer (*Odocoileus virginianus clavium*), with a total population of approximately 900, is an endangered species and is most concentrated on BPK (Villanova et al., 2017). Approximately 50% of the island area is designated as Key Deer National Wildlife Refuge (Langevin et al., 1998).

Our study area is located at the south-eastern side of BPK facing the Atlantic Ocean (Figure 1). Our sinkhole sites are located along a 350-m-long NNW trending transect. A sand berm with an elevation of ~0.5–1 m elevation forms a natural barrier from the Atlantic for the first sinkhole (Site 1), which is about 50 m from the beach and has very little surrounding vegetation. Sinkhole 2 (Site 2) is located ~100 m along the transect and is surrounded by mangroves. Sites 3 and 4 are 230 m and 350 m from shoreline, respectively, in dense shrub including buttonwood, Sea Grape Slash Pine, Gumbo Limbo, Poisonwood, and various cacti species. BPK is the only Key with multiple sinkholes thereby providing the opportunity to investigate changes in sedimentary characteristics as an extreme tropical cyclone's storm surge makes landfall.

To allow for the investigation of the sources of the foraminiferal assemblages found in the sinkholes, the inland transect was extended

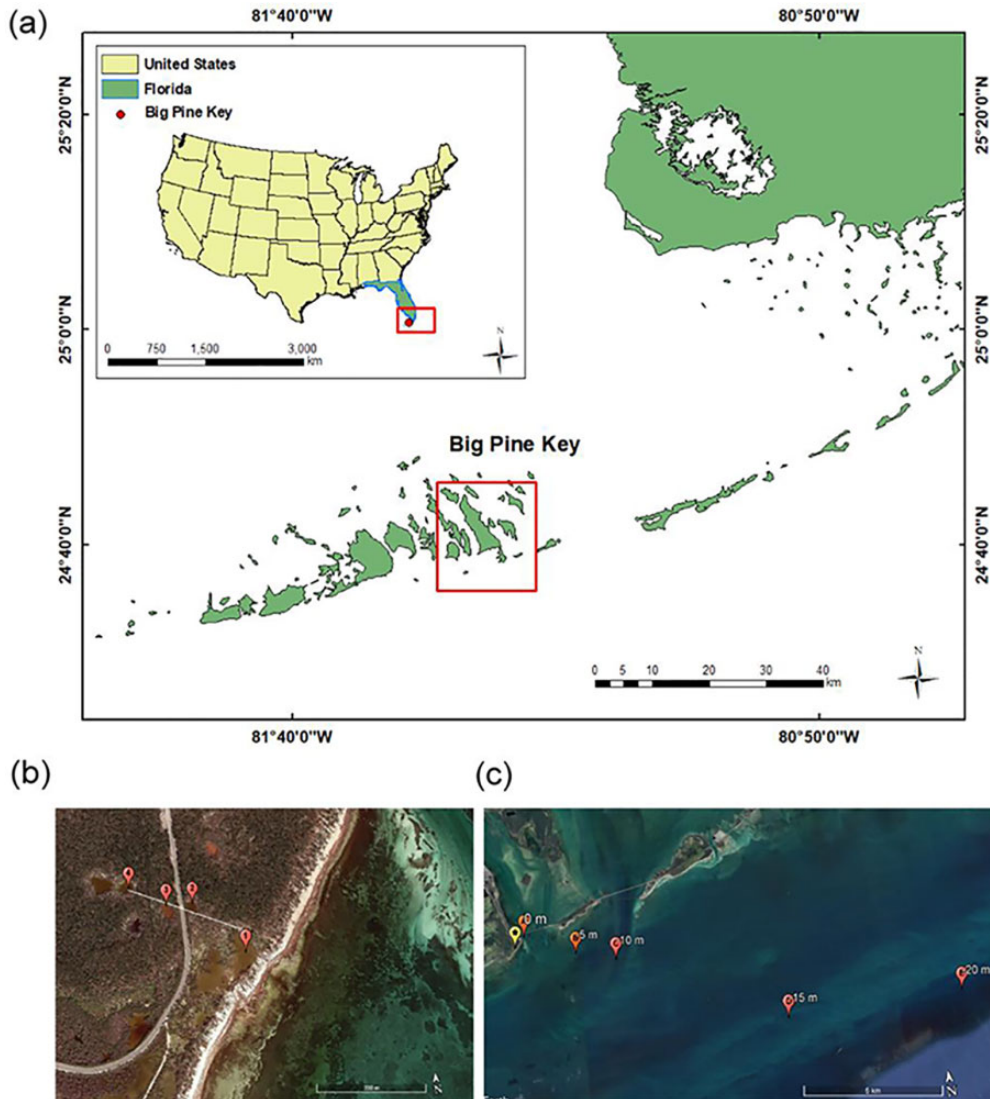


Figure 1. (a) The related location of US, Florida, and Big Pine Key; (b) the inland transect (white line) showing the sinkhole locations (red balloons 1–4); (c) the offshore transect with incremental 5 m of water depth to the edge of continental shelf (red balloons A–E). The yellow balloon is the location of inland study site. © Google Earth 2019.

16 km offshore to a depth of 20 m. Beyond this point the water depth increases rapidly as it is close to the edge of the barrier reef, and it is unlikely that the storm surge would have entrained sediments from deeper water along the steep-bottomed slope. Along this ESE bearing, sediment samples were collected using a

grab sampler at incremental depths of 5 m (Figure 1).

Hurricane Irma, a category 4 hurricane, made landfall at Florida Keys on 10 September 2017. It started as a tropical wave near the Cape Verde Islands on 30 August 2017. Fueled by the warm Atlantic waters, it became a category 5

Table 1. Sampling locations of offshore sediments.

Site	Coordinates	Water depth (m)	Offshore distance (km)	Distance from core sites (km)
1	−81.330° W, 24.646° N	0	0	0
2	−81.308° W, 24.638° N	5	1.0	2.3
3	−81.293° W, 24.634° N	10	2.2	3.8
4	−81.232° W, 24.620° N	15	6.8	10.7
5	−81.166° W, 24.606° N	20	9.7	17.0

hurricane and first made landfall on the Leeward Islands. By 8 September, the cyclone weakened to a category 4 hurricane and made landfall on Cudjoe Key on 10 September, which is only 15 km due west from BPK. The storm placed BPK in the right front quadrant of the hurricane with strong southeasterly winds as it made landfall. These southeasterly winds produced maximum storm-surge heights of up to 2.4 m (NAVD88) on the south and eastern shores of the island (Cangialosi et al., 2018; US Geological Society, 2017).

III Methods

3.1 Sample collection

From each of the four coastal sinkholes (sites 1–4), three cores were collected on 7 April 2018 on BPK using 76-mm-diameter acrylic tubes (total 12 cores), hand-pressed into the soft sediments. Florist foam was inserted into the top of the core to prevent disturbance of the surface sediment, and the core was capped top and bottom. Five offshore grab sediment samples were collected on the Atlantic side of BPK along an ESE transect at incremental depths of 5 m except for the most immediate nearshore sample, which is at 0 m (−5 m, −10 m, −15 m, and −20 m) (Figure 1(c) and Table 1). The GPS on the sampling vessel was used to keep to the ESE transect. However, in order to achieve the desired depth, which was measured with the boat's echo sounder, we shifted slightly off the ESE transect. Site E was close to the edge of the Florida

coral reef platform beyond which water depths increased rapidly.

Additionally, surface sediment (soil) samples surrounding each sinkhole were collected on the side closest to the Atlantic Ocean. These samples were collected to determine the source and extent of other contributing sediment found in the storm layers in the sinkhole. The trajectory of this inland transect follows the predominant wind direction of Irma as it approached BPK.

3.2 Sample analysis

Sinkhole core samples were analyzed for their sedimentary characteristics, grain size, short-lived radioisotope dating ($^{210}\text{Pb}_{\text{xs}}$), total organic matter, foraminiferal assemblages, and XRF spectrometry. The description of sedimentary characteristics included photographs, microscopic images, and Munsell color chart readings. These included sediment layering, shells, microfossils, and any other material (e.g., vegetations) contained in the sediments.

The short acrylic push cores were extruded at 5 mm intervals over the top 150 mm according to the methods of Schwing et al. (2016). Short-lived radioisotope geochronology was developed at 0.5 cm resolution for excess $^{210}\text{Pb}_{\text{xs}}$, ^{137}Cs , and ^7Be . Samples were run on GWL Series HPGe (High-Purity Germanium) Coaxial planar Photon Detectors at Eckerd College for total ^{210}Pb (46.5 keV), ^{214}Pb (295 keV and 351 keV), ^{214}Bi (609 keV), ^{137}Cs (661 keV), and ^7Be (447 keV) activities. Data were corrected for counting time, detector efficiency, and

geometry, as well as for the fraction of the total radioisotope measured yielding activity in dpm/g (disintegrations per minute per gram). Detector efficiency was determined using similar methods to Kitto (1991) using the IAEA 447 standard.

Cesium-137 is a thermonuclear byproduct and represents the period of greatest atomic bomb testing in the early-mid 1960s (Olsson, 1986). Berillium-7 has a very short half-life (~ 53 days) and is an indicator of recent sediment deposition (~ 1 year) and preservation of the core top. Excess ^{210}Pb ($t_{1/2} \sim 22.3$ years) is used for dating over the last ~ 100 years. The activities of ^{214}Pb (295 keV), ^{214}Pb (351 keV), and ^{214}Bi (609 keV) were averaged as a proxy for the ^{226}Ra activity of the sample or background ^{210}Pb . Background ^{210}Pb was subtracted from total ^{210}Pb to determine excess ^{210}Pb (Holmes, 2001). Excess ^{210}Pb data were input into the constant rate of supply (CRS) model to provide dating of each sample analyzed within the last ~ 100 years (Appleby and Oldfield, 1983; Binford, 1990). This was compared to ^{137}Cs data, an independent dating technique, to determine how well the CRS model was performing.

Total organic matter (TOM) was analyzed by the loss-on-ignition method, and samples were collected every 10 mm down the core to a depth of 70 mm. Each sample was placed in a ceramic crucible that was weighed and then dried at 105°C in a convection oven for 12 hours. This sample was reweighed and then heated at 550°C for 4 hours in a muffle furnace then placed in a desiccator to cool (Blume, 1990; Nelson and Sommers, 1996). LOI calculation shows as following equation (1) (Heiri et al., 2001)

$$\text{TOM} = ((\text{DW}_{105} - \text{DW}_{550}) / (\text{DW}_{105})) \times 100 \quad (1)$$

where DW_{105} is dry weight after 105°C heating and DW_{550} is dry weight after 550°C combustion.

For grain size analyses the sediment was sampled every 10 mm and wet sieved using the $63 \mu\text{m}$ sieve. With the fines of materials separated and weighted separately for the mud content, the sizes of the coarse sediment fraction were analyzed using standard sieves ranging from -4ϕ to 4ϕ at 0.25ϕ interval. The same sieving procedure was conducted on sediments collected from around the sinkholes and the offshore sites.

A diverse assortment of marine, benthic foraminifera in a discrete sediment layer can be a key indicator of storm transport suggesting the origin of the storm deposits (Gregory et al., 2015). Marine foraminifera differ in their tolerance to ambient light, which reflects ocean water depths (Hottinger, 1997). Consequently, the foraminiferal assemblages in a particular storm layer could suggest the cyclonic strength with more intense storms entraining foraminifera from deeper offshore environments (Haslett et al., 2000; Hottinger, 1997). In addition, the preservation indices of foraminifera relate to the depositional environment and the period of preservation. Live foraminifera transported from deeper waters during the storm may be slightly damaged but will not experience dissolution as this process occurs post-mortem (Boltovskoy and Totah, 1992; Wang and Chapell, 2001).

Foraminifera analyses were conducted to obtain information on sediment sources. The $63 \mu\text{m}$ sieved samples at 10 mm interval of core sediments and 30 g soils around the sinkholes were dried and up to 200 foraminifera tests per sample were collected and identified to genus level (Hallock et al., 2003) following the taxonomy of Loeblich and Tappan (1987). Foraminifera collected from the sediments were compared with those from the nearshore environment for Florida as described in the literature (Arribas et al., 2007; Loeblich and Tappan, 1987; Murray, 2014). In addition, foraminiferal assemblages were analyzed by using a variety of non-metric multidimensional scaling (NMDS)

ordination methods with Paleontological Statistics Program (PAST v4.03: Hammer, 2012), minimum sample sizes ($n \geq 10, 15, 25, \text{ or } 50$), similarity metrics (Euclidean or Bray-Curtis), and data transformations (proportional, square root, or log abundance). NMDS is a widely used method of multivariate statistical analysis for presenting species composition and the similarities of data. Data transformation could moderate the effects of dominant taxa to mitigate the potential influence of taphonomic bias (Clarke et al., 2014).

Finally, sinkhole cores were analyzed with an XRF spectrometer at the University of Miami for detecting elemental changes in the core profiles. Cores were scanned at 10 kV (detecting light elements Mg to Rh) and 30 kV (detecting heavier elements Ni to Bi) with a pitch of 10 seconds and 15 seconds, respectively, at 200 mA. The resolution of detection was set at 5 mm as down-core direction. The elemental signals of soil samples from around the sinkholes and offshore samples were measured with a TRACER 5i portable XRF spectrometer in the Laboratory for Archaeological Science, Department of Anthropology, University of South Florida. Samples were analyzed for 20 seconds using a helium flow, with settings of 10 kV and 35 μA and no filter, for elements Mg through Fe, and for 30 seconds with settings of 50 kV and 35 μA and using a filter to minimize background and enhance detection for elements Ca through Nb.

IV Results

4.1 Chronology and sediment stratigraphy

The chronologies of the upper 70 mm of each sinkhole core, using ^7Be , $^{210}\text{Pb}_{\text{xs}}$, and ^{137}Cs dating, are documented in Table 2. Based on the sediment linear accumulation rate and the sediment mass accumulation rate, all sinkholes except the furthest from the coastline (core 4), have sediments that correspond with the timing of Irma making landfall on BPK.

Table 2. The chronology of the upper 7 cm of the sinkhole cores 1–4 (Irma year is marked in bold).

Depth (cm)	Core 1 age (yr)	Core 2 age (yr)	Core 3 age (yr)	Core 4 age (yr)
0–1	2018.4	2018.0	2017.7	2014.1
1–2	2018.1	2017.7	2017.7	2012.0
2–3	2017.7	2017.7	2017.7	2010.3
3–4	2017.7	2015.3	2017.7	2009.1
4–5	2017.7	2012.1	2016.0	2007.4
5–6	2017.7	2005.4	2015.9	2005.1
6–7	2017.7	2001.2	2015.9	2004.8

Photographic images of the upper 15 cm for each core reveal distinct variations in the stratigraphy of the sinkhole sediments (Figure 2). The uppermost layer of core 1 is a brown sandy mud with a thin green alga layer. The top 1 cm of core 2 has similar characteristics. The depth 3–7 cm of core 1 consists of poorly sorted sand and shell fragments, and from 7 cm to 15 cm is well sorted as a brown gray (Munsell color: 2.5Y 6/2) lime mud (Figure 2(a)). There is a sand layer around 1–3 cm in core 2, and beneath 6 cm is a layer of dense mud (Figure 2(b)). The top 0–6 cm of core 3 is composed of moderately sorted, viscous, muddy sand that includes snails and wood pieces (Figure 2(c)), and the color presents much lighter (10YR 4/2) than the rest of the fine sediments (2.5Y 6/2). In addition, characterized by uniform mud, there is little difference in the sediments between the upper and lower layers of core 4 (Figure 2(d)).

The microscopic images (Figure 2) of the Irma layer sediments (top ones) for sinkholes 1–3 are coarser than the lower non-Irma layers. A closer inspection of the Irma layers shows larger grain size, shell fragments, and poor sorting. Below this layer, the sediments are much finer, with a clay/mud consistency. There is little difference in the sediments between the upper and lower layers for sinkhole 4, which is not surprising, as there are no overwash sediments in the sinkhole.

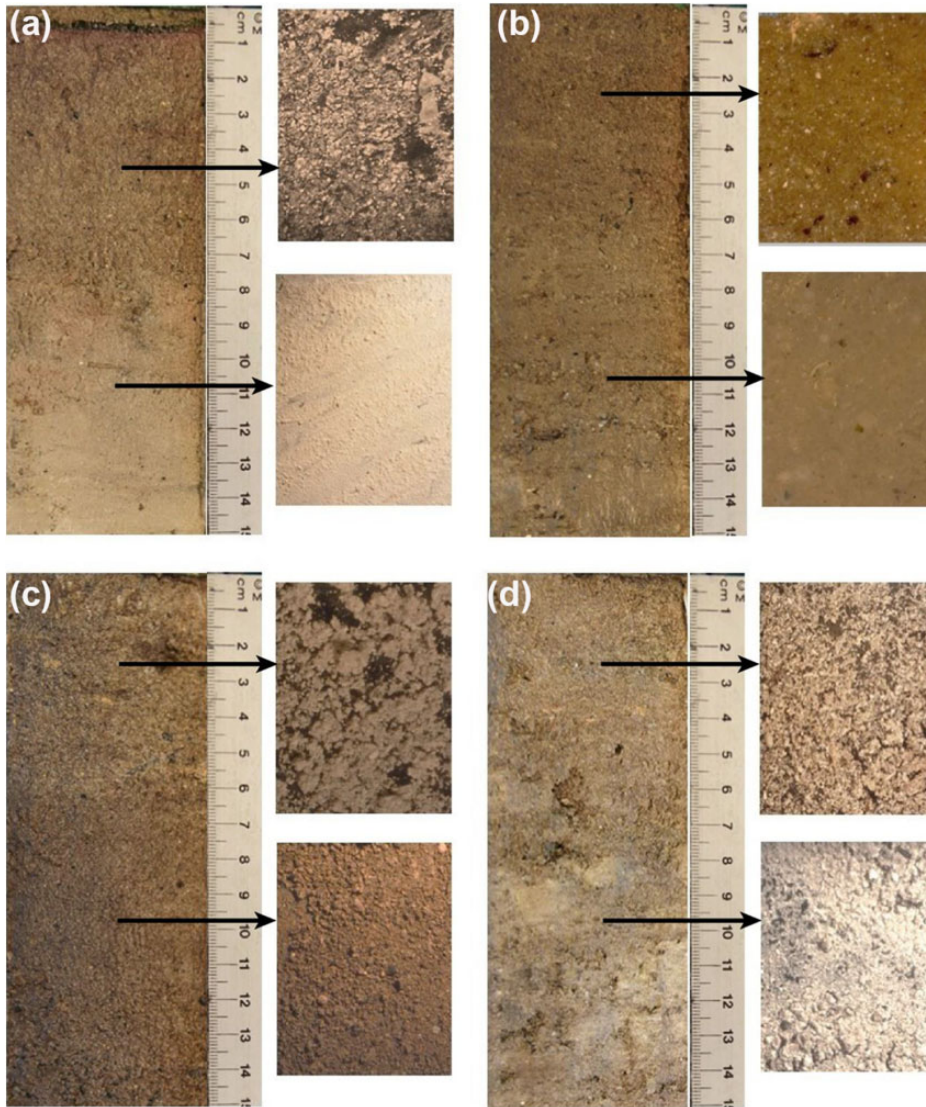


Figure 2. (a–d) The stratigraphy of cores 1–4, respectively. Irma deposits are 1–7 cm in core 1 (a), 2–3 cm in core 2 (b), and the upper 4 cm in core 3 (c). The Irma layers in core 2 show a subtle change in sediment characteristics which are more discernible in microscopic image. Core 4 (d) does not contain Irma deposits. The hole in core 3 at 2–3 cm is from the removal of a large shell. Microscopic images of the Irma and pre-Irma sediments for sinkholes 1–3 to the right side of each core. The top and bottom of sinkhole 4 are both pre-Irma sediments. Samples were disaggregated in water within a petri dish to allow photographing of the samples with a magnification of 25 \times .

4.2 Total organic matter (LOI) and grain size analysis

The chronology of each core shows which sediments are pre/post-Irma and Irma deposits

(Table 2). These age controls allow for the determination of the differences in TOM and water content of the Irma and non-Irma sediments (Figure 3). The Irma layers are characterized by lower organic content, with averages of

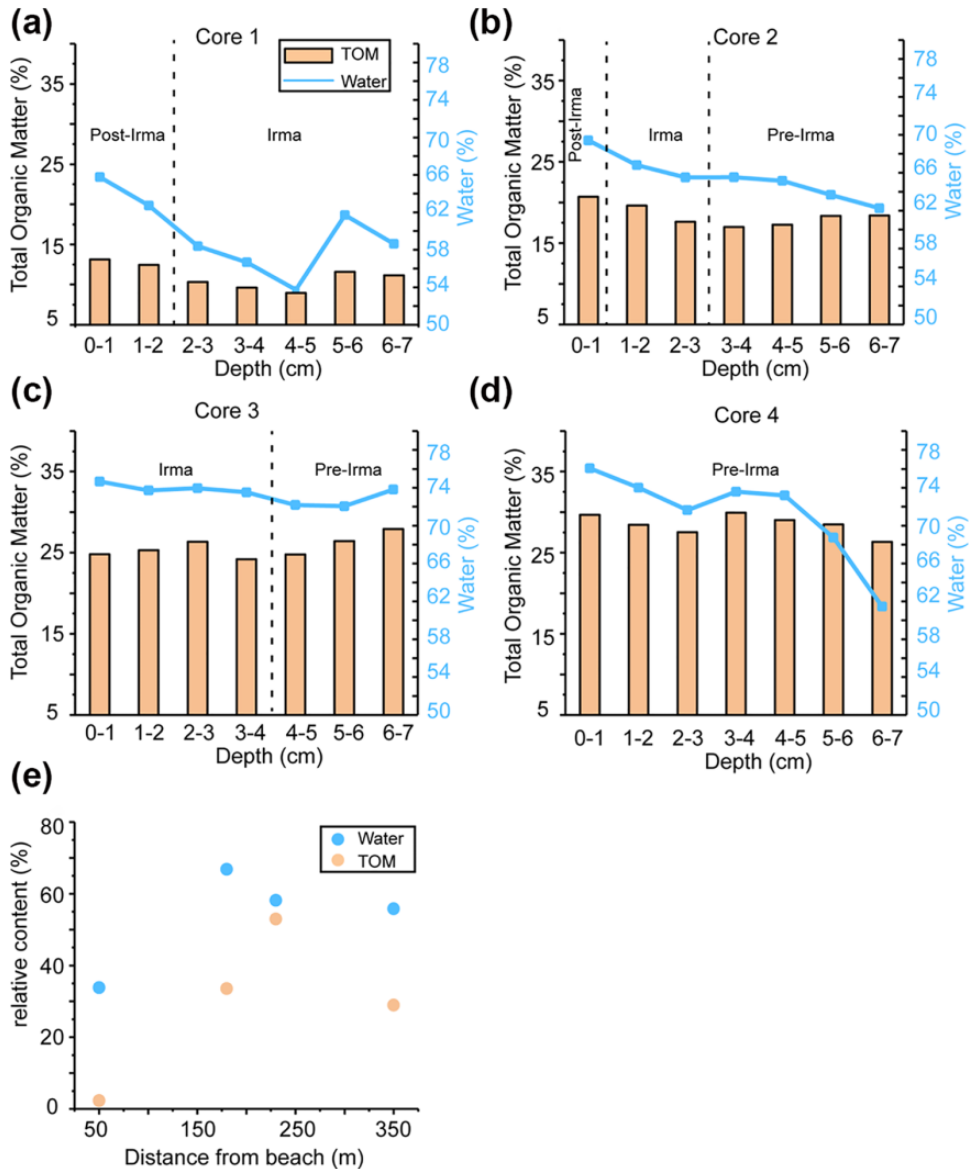


Figure 3. (a–d) Total organic matter and water content (%) of top 70 mm of cores 1–4; (e) total organic matter and water content of soils surrounding the sinkholes.

11.03%, 18.43%, and 25.69% for cores 1–3, respectively, and lower water contents. The pre/post-Irma deposits contain more organic matter than Irma layers in cores 1–3. Core 1 shows a distinct difference, while core 2 and core 3 show slight differences in TOM. Although core 4 contains the highest TOM at

29.93%, this core does not contain Irma deposits. Of the soil samples, sites 2–4 contain greater amounts of TOM, with up to 52.99% for site 3 (Figure 3(e)).

Grain size distributions of the core samples, surrounding soil samples, and offshore grab sediments are shown in Figure 4. D90 (90% of

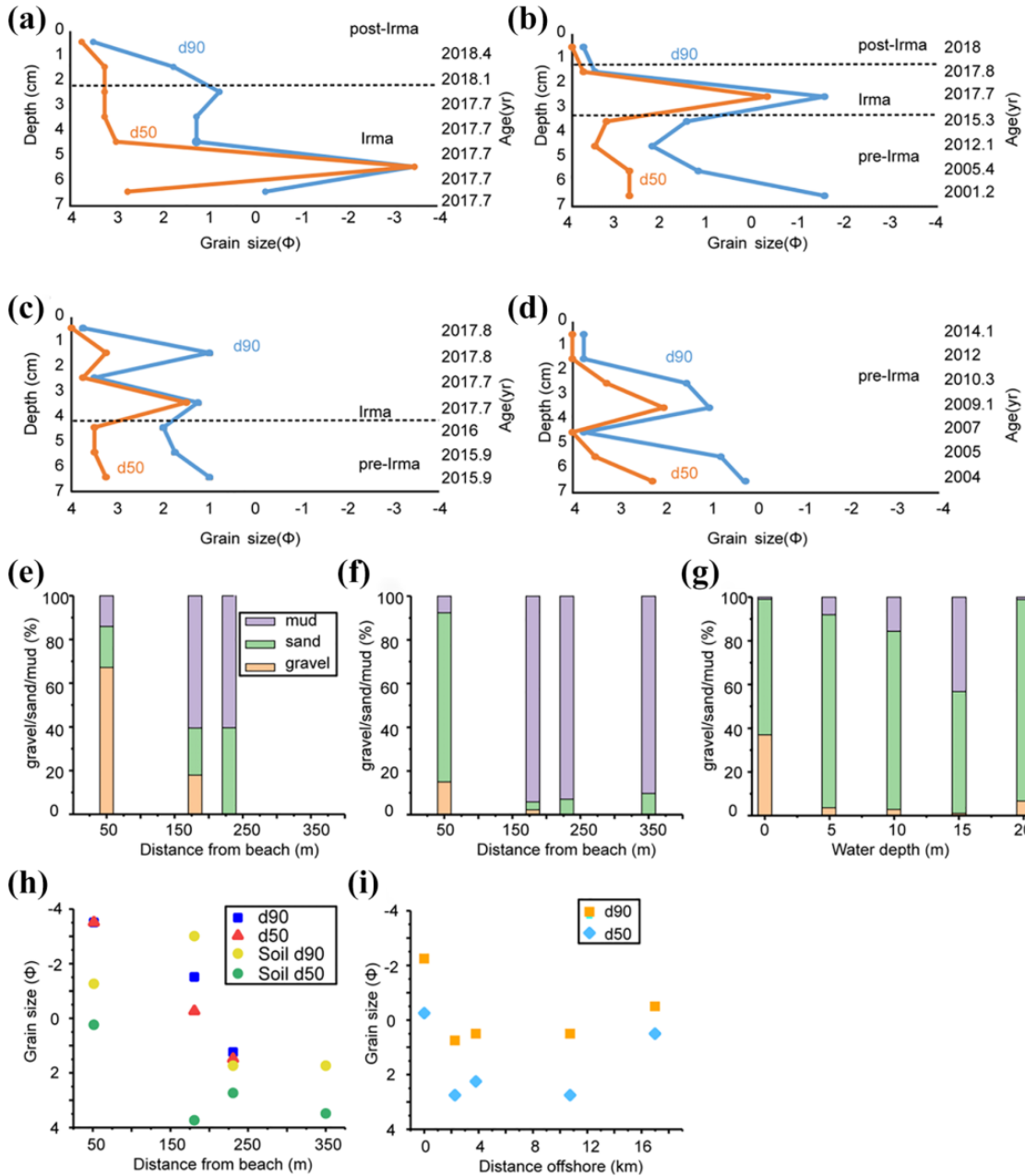


Figure 4. (a–d) Grain size distribution for core 1–4, respectively, and the chronology of the upper 70 mm; (e) grain size compositions of the coarsest Irma layers of cores 1–3 (from left to right); (f) grain size compositions of the soils surrounding sinkholes 1–4 (from left to right); (g) texture compositions of offshore sediments; (h) grain size distribution of the coarsest Irma sediments of cores 1–3 (blue d90 and red d50), and sinkholes 1–4 surrounding soils (yellow soil_d90 and green soil_d50). The values of d90 and d50 core 1 coarsest overwash sediment are the same, so they overlap. Core 4 does not have d90/d50 data because of non-Irma deposits; (i) grain size distribution for offshore sediments (orange offshore_d90 and light blue offshore_d50) with the different distance away from the beach. Different distances correspond to different sites (Table 1).

particles smaller than this diameter) and d50 (50% of particles smaller than this diameter) define the sand size distribution to allow for the comparison of core sediments and other sedimentary sources as shown in Figure 4(a–d). The Irma sediments of cores 1–3 present abrupt peaks of both d90 and d50, showing the coarser grain size than the pre/post-Irma sediments (Figure 4(a–c)). The whole core 4 contains pre-Irma sediments, for which the grain size is finer than 1 mm and much smaller than Irma sediments.

At 6 cm in core 1, the deposits are coarsest with 67.18% gravel (the diameter size > 2 mm), 18.81% sand (2 mm > the diameter size \geq 0.063 mm), and 14.01% muds (the diameter size < 0.063 mm) (Figure 4(e)). Gravel deposits (17.92%) are also found in core 2 at a depth of 3 cm, and 21.58% of sand in Irma layer is much greater than the post/pre-Irma (Figure 4(e)). Although there are no gravel deposits in core 3, the sand percentage in Irma layer has an abrupt increase to 39.61 (Fig. 4(e)). Most of core 4 sediments are mud, up to 80.20–95.78% (dry weight%), with some sand at 0.35–2.16%.

The soil sample from site 1 has a much higher sand percentage (77.38%, Figure 4(f)) and more gravel (14.99%) than more inland sites due to it being only 50 m from the beach. The soils surrounding the remaining sites are overwhelmingly organic rich muddy soils with little sand (Figure 4(f)). Sand is the dominant sediment in the offshore sediments with up to 92.16% at depth 20 m (Figure 4(g)). Only the nearshore sediments contain significant amounts (36.99%) of gravel (containing broken shells). A surprising result is the 43.20% mud content of sediments at depth 15 m, which is dissimilar to other offshore sediments.

The grain size distributions of d50 and d90 at 6 cm in core 1 and 4 cm in core 3 are very similar indicating that the gravels/sand portion of the sediments is very well sorted, and it is strong evidence of storm deposits (i.e., sorting

by the storm waves) (Figure 4(h)). Although there is a large difference between d50 and d90 of core 2, the sand portion presents very similar grain sizes, while the gravel weights influence the result of the d90.

In general, the particle size of the coarsest Irma sediments of cores 1–3 are larger than the surrounding soils (Figure 4(h)). The grain size of core 4 is fine with a high concentration of mud, and the surrounding sediments are even more finely grained. Comparatively, the grain size distribution of the offshore sediments (at depth 5, 10, 15 m) is very similar with the nearshore sediments being the coarsest (Figure 4(i)). Contrasting Figure 4(h) with Figure 4(i), the coarsest Irma deposits of cores 2 and 3 are like the offshore sediments. Although the largest fraction of the Irma deposits of core 1 are very coarse due to the high content of gravel, the sand size of the Irma layers of cores 1–3 are like those of the offshore sites.

4.3 Foraminifera analysis

There is a high level of diversity in the foraminiferal assemblages in the Irma layers with 23 different foraminiferal species (Figure 5). Most show good preservation (> 95%), suggesting that they were deposited very recently by a singular event. These different species are from shallow marine (high-salinity tolerant) environments, suggesting transport from the Atlantic via storm-induced sediment mobilization (Figure 6).

The total number of foraminifera vary greatly within the layers of each core (Figure 7). Cores 1–2 yield abundant benthic foraminifera for the Irma deposits compared to the non-Irma deposits (Figure 7(a–b)), whereas the number of benthic foraminifera in core 3 (Figure 7(c)) decreases to approximately 50 specimens in the Irma sediments and only five very small foraminifera are found in core 4 (Figure 7(d)). In addition, the number of total foraminifera in each layer decreases along the inland transect.

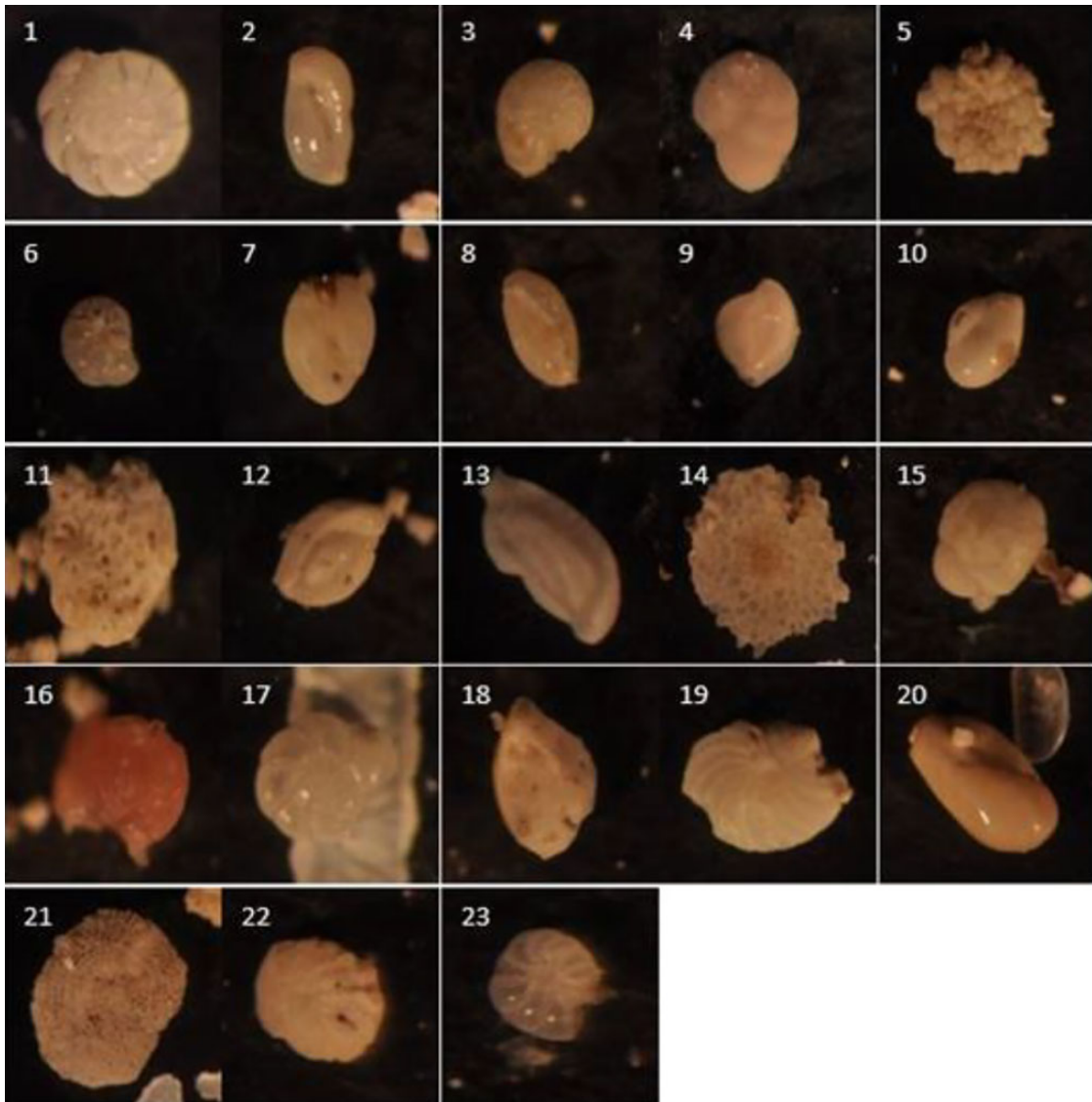


Figure 5. Foraminifera assemblages were found in Irma layers of the cores at Big Pine Key: 1. *Ammonia* sp. 2. *Quinqueloculina* sp. 3. *Elphidium* sp. 4. *Elphidium* sp. 5. *Planorbulina* sp. 6. *Elphidium* sp. 7. *Triloculina* sp. 8. *Triloculina* sp. 9. *Quinqueloculina* sp. 10. *Quinqueloculina* sp. 11. *Elphidium* sp. 12. *Quinqueloculina* sp. 13. *Siphonaperta* sp. 14. *Planorbulina* sp. 15. *Planulina* sp. 16. *Discorbis rosea*. 17. *Ammonia* sp. 18. *Spiroloculina* sp. 19. *Peneroplis* sp. 20. *Triloculina* sp. 21. *Sorites marginalis*. 22. *Elphidium* sp. 23. *Elphidium* sp. Magnification at 50 \times .

High abundances of well-preserved foraminifera belonging to 23 taxa are identified in Irma layers compared to low abundances for non-Irma sediments (Figure 7(a-d)).

The dominant species in the Irma layers of cores 1–3 are *Ammonia* spp. (*A. parkinsoniana*, *A. beccarii*, *A. tepida*, and *A. takanabensis*), *Elphidium* spp. (*E. galvestonense*, *E. sagrum*,

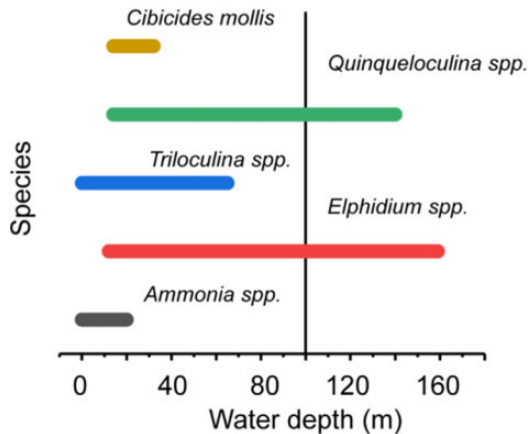


Figure 6. The length of the lines presents the various depths of different live foraminifera habitats of marine environments in the Atlantic (Murray, 2014; Orbigny, 1839).

E. advenum, *E. discoidale*, *E. excavayum*, and *E. fimbriatulum*), *Quinqueloculina* spp. (*Q. bicostata*, *Q. agglutinans*, *Q. lamarekiana*, *Q. carinata*, and *Q. laevigata*), and *Triloculina* spp. (*T. oblonga*, *T. linneana*, and *T. tricarinata*) (Table 3). Most of these are common in shallow marine water (about 0–50 m water depth, Figure 6) in the Atlantic Ocean (Felder and Camp, 2009; Murray, 2014; Orbigny, 1839; Wilson, 2006). The assemblages in the Irma layers of core 1 have the highest diversity and quantity of foraminifera, whereas the Irma layers of core 2 and core 3 are strongly dominated by *Ammonia* spp., 74% and 40%, respectively (Table 3). Otherwise, the quantity and diversity of foraminifera in non-Irma layers of cores 1–3 have dropped significantly, as *Ammonia* spp. (96.60%) dominated in non-Irma layers of core 2 and *Quinqueloculina* spp. (86.67%) in non-Irma layers of core 3.

Owing to the frequent exposure to the hard bottom of the carbonate-dominated shelf/reef offshore BPK, the numbers of living foraminifera were low in offshore sediments. Of those, *Ammonia* spp., *Elphidium* spp., and *Quinqueloculina* spp. were most common. In addition,

there were no foraminifera found in the soils surrounding the sinkholes.

4.4 XRF spectrometry

Of 29 elements measured by the XRF analyses, only Si, Al, Ca, Ti, and Fe provided clear differences among the various sites (Figure 9). The highest Si/Al ratios are present in the Irma sediments (cores 1–3), which are considerably higher than soils surrounding the sinkholes (sites 1–3) and the offshore sediments (Figure 9: A–E). It is also noteworthy that this Si/Al ratio increases landward along the sinkhole transect. The offshore sediments have comparatively higher Ca/Ti ratios, and there is a decrease along the sinkhole transect. The soils surrounding the sinkholes have very low ratio values. Finally, in comparison to the offshore sediments, Fe/Ca ratios are highest in the terrestrial locations with the soils and Irma deposits having similar ratios except for site 3.

V Discussion

5.1 A conceptual model

Figure 10 provides a conceptual model reconstructing the events that arose from a major hurricane making landfall on a carbonate environment that is punctured by sinkholes that act as traps for storm-surge-entrained sediments. Sand layers and shell fragments in the sediment cores of coastal lakes and marshes have been attributed to high-energy storm events depositing marine sediments (overwash) from the nearshore environment (González-Regalado et al., 2019; Lane et al., 2011; Liu and Fearn, 2000; Yao et al., 2020). Based on the ^{7}Be , ^{210}Pb , and ^{137}Cs chronology, these characteristic layers are present in the sinkholes 1–3, which correspond to the landfall of Hurricane Irma on BPK. These overwash layers of coarser material are below (sinkhole 1) and above (sinkholes 2 and 3) sediments rich in organic matter. Additionally, Irma's overwash layers have very

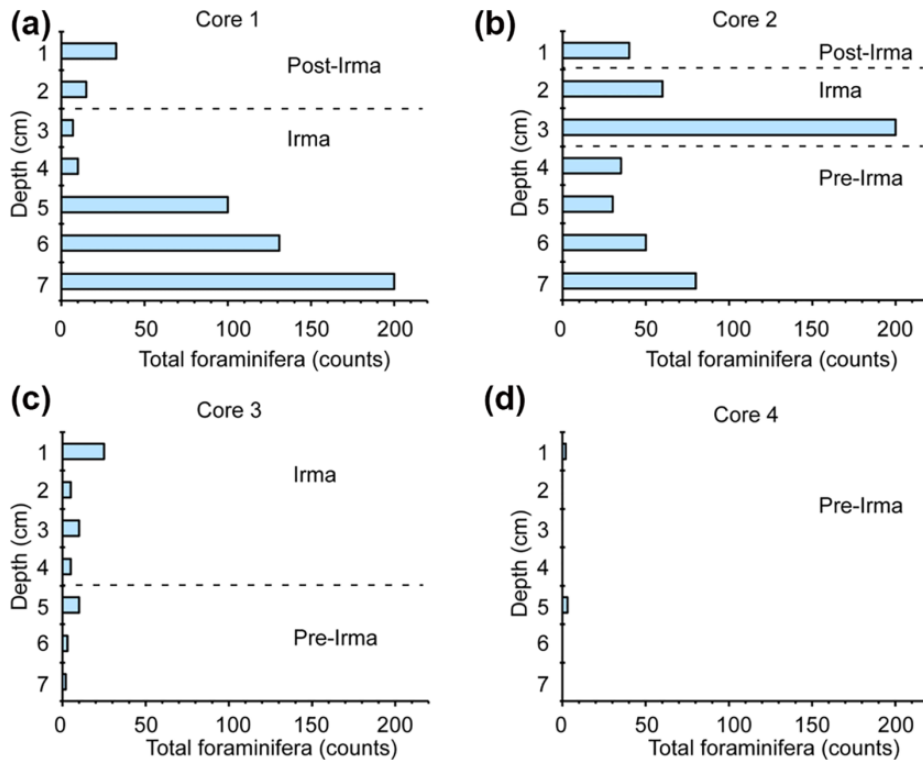


Figure 7. (a–d) Total foraminiferal counts at each centimeter depth of cores 1–4. Non-metric multidimensional scaling (NMDS) analysis of foraminiferal assemblage abundances shows a clear consistency of the groupings (see Figure 8). In particular, the three Irma layers of core 1 all have highly consistent foraminiferal abundances which are very different from the post-Irma layer. These results suggest no mixing in the Irma layers and that the foraminifera all have the same marine origin. The post-Irma and uppermost pre-Irma layers of core 2 at depth 4 cm are similar to the Irma layers. The high values of *Ammonia* spp. in all these layers indicate potential mixing. In addition, although the stratigraphically lower pre-Irma layers of core 2 and the very top Irma layer of core 3 show highly consistent similarities, they do not have identical species abundances, implying that there are less Irma sediments deposited in sinkhole 3. Other layers where the sample size is smaller than 25 individuals are not presented in this figure.

Table 3. The percentage of dominant foraminifera species in Irma and non-Irma layers of cores 1–3.

Species (%)	Core 1		Core 2		Core 3	
	Irma	Non-Irma	Irma	Non-Irma	Irma	Non-Irma
<i>Ammonia</i> spp.	33.99	12.50	73.85	96.60	40.00	-
<i>Elphidium</i> spp.	14.06	14.58	9.23	-	6.66	-
<i>Quinqueloculina</i> spp.	23.58	29.17	13.08	1.28	33.56	86.67
<i>Triloculina</i> spp.	10.66	39.58	1.92	-	17.78	-
<i>Cibicides mollis</i>	5.67	-	-	-	-	-
Others	12.24	4.17	1.92	2.12	-	13.33

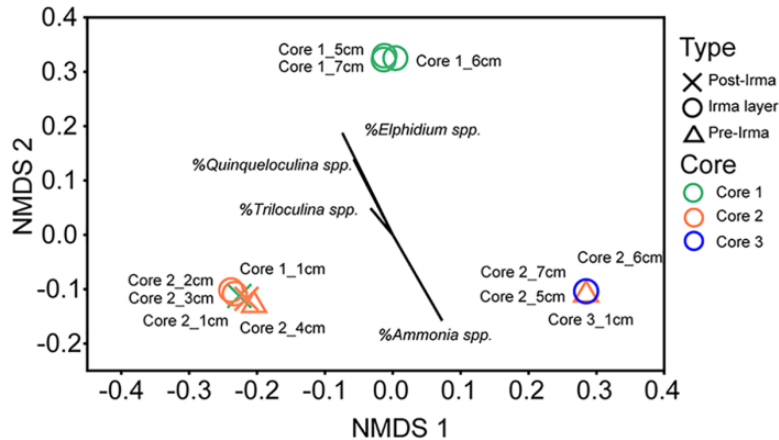


Figure 8. Non-metric multidimensional scaling (NMDS) analysis of foraminiferal assemblage abundances using Bray–Curtis similarity index and proportional data transformation; minimum individuals per sample $n \geq 25$.

different sediment characteristics than the soils surrounding the sinkholes (Figure 4(e–g)).

As storm surges and storm waves move ashore, they lose energy and entrainment capability (Möller et al., 2014; Shepard et al., 2011), which suggests that the thickest overwash layers should be in the sinkholes closest to the coast (Figure 10). It clearly shows this thinning in the Irma sinkhole sediments with core 1 having at least 5 cm of overwash compared to 4 cm for core 3. The furthest inland site, sinkhole 4, does not contain any Irma sediments.

Studies have found that foraminifera species type and taphonomic composition can show the origin of storm deposits and distance of transport (Pilarczyk et al., 2012, 2014; Tanaka et al., 2012). The high abundances of foraminifera in the storm layers of the sinkholes match the high-energy event that was Irma whose storm surge transported and deposited foraminifera of marine origin into the sinkholes. For example, *Archaias angulatus* (Fichtel and Moll, 1803), which are found at a depth of 6–7 cm of core 1, can be found in water depths of 0 m to at least 30 m (Wilson, 2006). These foraminifera species cannot survive in anoxic sediments of the sinkholes so

can only be deposited by storm overwash. The increased frequencies of *Elphidium* spp. combined with *Ammonia* spp. also provide evidence of marine sediment overwash (Arribas et al., 2007). Other species can only be found in the various depths of marine environments of the Atlantic continental shelf of Florida Keys: *Ammonia* spp. (0–20 m), *Elphidium* spp. (12–159 m), *Triloculina* spp. (0–65 m), *Quinqueloculina* spp. (14–140 m), and *Cibicides mollis* (14–32 m) (Murray, 2014; Orbigny, 1839) (Figure 6). However, the multivariate analyses (NMDS) demonstrate that not all the sinkholes have definitive Irma layers. The NMDS for sinkhole 2 showed signs of sediment mixing. A possible explanation for this mixing is the sinkhole’s proximity to the road embankment. As the storm surge came ashore, it passed over sinkhole 1 without any resistance, but when it came to sinkhole 2, the impediment created by the road would have produced some backwash leading to turbulence and therefore mixing of the Irma and non-Irma sediments. Overall, the type of species present in the sinkholes suggest that Irma entrained sediments from the offshore sediments of BPK. The progressive decrease of the

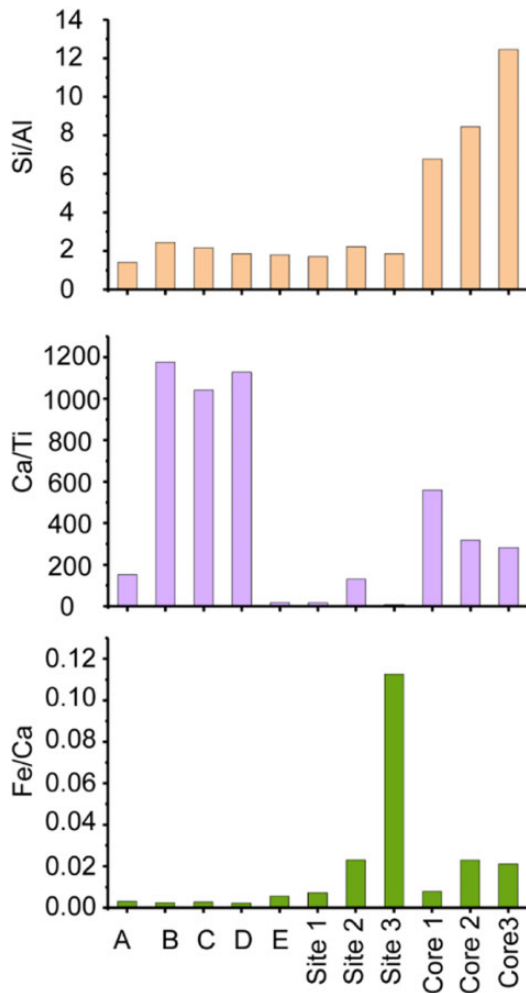


Figure 9. XRF analyses for offshore sediments (A–E represent the depth from 0 to 20 m), surrounding soils of sinkholes 1–3 (sites 1–3), and the median value of Irma layers of cores 1–3.

abundance and variety of foraminifera along the transect helps confirm our conceptual model.

High levels of Ca have been attributed to marine sources (Liu et al., 2014; Ramírez-Herrera et al., 2012) and Ti having terrigenous origins (Riou et al., 2020; Yao et al., 2020). The high Ca/Ti values in the Irma layers represent offshore sediments and degraded bedrock compared to the relatively low values of non-storm

layers. The lesser Irma influence can be seen in the gradual decline in the Ca/Ti ratios along the sinkhole transect (Figure 9, middle panel). High Si/Al ratios in coastal lacustrine environments have been found by previous studies to represent storm deposits (Liu et al., 2014; Oliva et al., 2018). The high Si/Al ratios are present in Irma layers of cores 1–3. One possible source are diatoms, which are a source of biogenic silicate (Ehrenhauss et al., 2004). However, the investigation of the presence of diatoms was beyond the scope of our study.

5.2 Contribution of surrounding soils/sediments to storm layers

The results of the grain size, TOM analyses, and foraminiferal analysis provide an indication of the contribution of other sources of sediment besides that of marine origin. It is likely that a high-energy event such as Irma would also entrain the sediments (soils) that surround the sinkholes. Our results showed there were significant amounts of coarse material such as gravels, sand, shell fragments, and plant debris in the Irma layers. The percentages of TOM of soils surrounding sinkholes 1–3 are greater than those in the Irma layers, although the percentage of TOM is closest to the Irma deposits at sinkhole 2 (Figure 3). These could indicate that the surrounding soil contributed more sediments to the Irma layer at sinkhole 2, whereas Irma layers in sinkholes 1 and 3 contained more marine or other sources. Grain size analysis reveals that only 6–7 cm of core 1 and 3 cm of core 2 have significant increases of the coarser fraction (gravel). Otherwise, the size fraction (d₅₀) of Irma layers in sinkholes 1 and 3 is composed of offshore sediments, while in sinkhole 2 it is similar to its surrounding soil. Consequently, we can determine that Irma deposits in sinkholes 1 and 3 were transported from more marine sediments rather than surrounding soils, while sinkhole 2 entrained more surrounding soil, which could be caused by the different

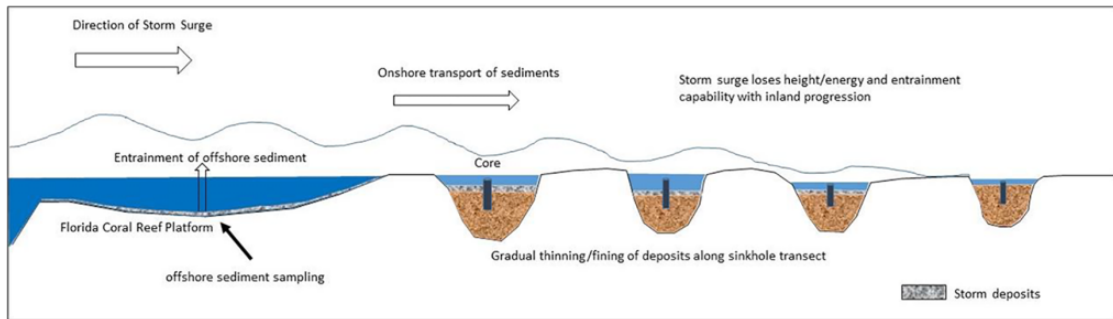


Figure 10. Conceptual model of events created by a major hurricane making landfall in a carbonate environment containing coastal sinkholes.

surrounding environments of sinkholes. Although sinkhole 2 is closer to the coast than sinkhole 3, there are dense shrubs surrounding sinkhole 2 and a steeper embankment on the roadside than the slope leading to the road for sinkhole 3. Sinkhole 1 is closest to the coast, and there is the smooth surface of a road in front of sinkhole 3, so that they have more open space to allow easier passage of Irma's storm surge and entrained sediments. Therefore, the immediate surrounding environment, especially the vegetation density, also have a significant influence on the storm deposits within the sinkholes.

The low concentration of Fe in the storm sediments can be an indicator of storm overwash (Chagué-Goff et al., 2000). Decreasing Fe/Ca values are associated with the sediments containing high shell content (Jiménez-Berrocso et al., 2004), which are found in the Irma layers. Conversely, high Fe/Ca ratios in sinkholes could be indicative of elevated Fe concentrations that are a product of redox reactions in the sediments due to low oxygen levels (Sun Loh et al., 2013). The non-Irma deposits were rich in organic material and had a strong sulfur smell. These characteristics suggest an anoxic environment which is conducive for the redox reactions increasing the Fe content of the sediment.

High Fe/Ca in soils and sinkholes and low values in marine sediments suggest that the

surrounding soil was entrained by storm surge and deposited with sediments of marine origin. This indicates the contribution of soils to Irma deposits for sinkholes.

5.3 Bioturbation of the sinkhole sediments

In general, bioturbation refers to the displacement and mixing of sediments by fauna/flora (Sturdivant et al., 2012). Dissolved oxygen concentration is significantly related to bioturbation, and hypoxic environments are not conducive to fauna that are responsible for this process that disturbs the sediments. The strong sulfur smell of the sinkhole sediments indicates hypoxia. Sinkholes (karst basin) usually have an anoxic bottom environment due to the limitation of water circulation (Gregory et al., 2017). Therefore, sediments in sinkholes are unlikely environments for bioturbation, and the clear transitions of the foraminifera in the Irma layers provide further evidence on this conclusion (Savrda et al., 1984). Intense bioturbation often destroys sediment layering in storm overwash deposits. Therefore, weak bioturbation within sinkholes provides a favorable condition for the preservation of storm deposits.

VI Conclusions

Here we provide the infrequent/valuable paleotempestology record of a major tropical cyclone

for a carbonate environment on the Atlantic coast of the USA, specifically the Florida Keys. In particular, we investigate the potential of sinkholes as reliable records of extreme storms. The category 4 tropical cyclone that provided the storm deposits was Hurricane Irma, which made landfall just south of our study area, Big Pine Key. In addition to investigating evidence for this hurricane in the sinkholes, we also attempt to determine their various sources, being that of marine or terrigenous origins.

Based on our ^7Be , $^{210}\text{Pb}_{\text{xs}}$, and ^{137}Cs constructed chronology, we determined that our sinkhole sediments correspond to the landfall of Hurricane Irma in September 2017. Core description, sediment grain size analysis, TOM, microfossil analysis, and XRF are all inexpensive and reliable methods for detecting storm events. Our sedimentary record of Irma showed: (1) the fine organic rich muds were replaced by coarser marine sediments (increase in grain size); (2) TOM decreased for the storm deposits as the organic matter produced within and around the sinkholes was replaced by the inorganic marine sediments; (3) abundant and diverse marine foraminifera were found in Irma layers, notwithstanding some mixing in core 2, while the diversity and quantity tapered off along the transect; and (4) Si/Al and Ca/Ti ratios provided evidence of the marine contribution for the storm sediments and the Fe/Ca ratios demonstrated the additional surrounding soils entrained by the storm surge.

We propose that sinkholes are reliable depositories for storm deposits. There is evidence of discrete storm layers with little evidence of significant bioturbation. The use of a transect of sinkholes illustrates the influence of distance from the coast as the storm deposits became progressively thinner. Finally, as there are many carbonate tropical locations in the Caribbean with coastal sinkholes, there exists a significant potential for future paleotemperature studies in these environments.

Acknowledgements

This research was supported by Dr. van Beynen and by the Tharp Research Endowed Scholarship, School of Geosciences, University of South Florida, Tampa, FL USA. We are grateful to Dr. Larry C. Peterson, University of Miami, for his support of XRF core scanning. We thank Dr. Pamela Hallock Muller, College of Marine Science, University of South Florida, for guiding foraminifera analysis. We also thank Dr. Arsum Pathak and Xiang Cheng for field sample collecting. Many thanks to the anonymous reviewers for their time and valuable comments.

Author contribution

This project was conceptualized by Dr. van Beynen and Youzhu Wang. Wang conducted the research and wrote the initial draft. Figures and tables were created by Wang and van Beynen. The interpretation of core description and grain size analysis was guided by Dr. Ping Wang. The chronology of the cores was produced under the advisement of Dr. Brooks. The interpretation of the foraminiferal analysis was performed by Dr. Herbert and Wang. The XRF data of soils was measured by Dr. Tykot. All authors reviewed and edited the final paper.


Declaration of conflicting interests

The author(s) declared no potential conflicts of interest with respect to the research, authorship, and/or publication of this article.

Funding

The author(s) received no financial support for the research, authorship, and/or publication of this article.

ORCID iD

Youzhu Wang  <https://orcid.org/0000-0002-2824-6323>

References

- Adomat F and Gischler E (2017) Assessing the suitability of Holocene environments along the central Belize coast, Central America, for the reconstruction of hurricane records. *International Journal of Earth Sciences* 106(1): 283–309.

- Appleby P and Oldfield F (1983) The assessment of ^{210}Pb data from sites with varying sediment accumulation rates. *Hydrobiologia* 103(1): 29–35.
- Arribas J, Critelli S and Johnsson MJ (2007) *Sedimentary Provenance and Petrogenesis: Perspectives from Petrography and Geochemistry*. Boulder, CO: Geological Society of America.
- Atwater BF, Fuentes Z, Halley RB, et al. (2014) Effects of 2010 Hurricane Earl amidst geologic evidence for greater overwash at Anegada, British Virgin Islands. *Advances in Geosciences* 38: 21–30.
- Bhatia K, Vecchi G, Murakami H, et al. (2018) Projected response of tropical cyclone intensity and intensification in a global climate model. *Journal of Climate* 31(20): 8281–8303.
- Bilskie MV, Hagen S, Medeiros S, et al. (2016) Data and numerical analysis of astronomic tides, wind-waves, and hurricane storm surge along the northern Gulf of Mexico. *Journal of Geophysical Research: Oceans* 121(5): 3625–3658.
- Binford MW (1990) Calculation and uncertainty analysis of ^{210}Pb dates for PIRLA project lake sediment cores. *Journal of Paleolimnology* 3(3): 253–267.
- Blume LJ (1990) *Handbook of Methods for Acid Deposition Studies: Laboratory Analyses for Soil Chemistry*. Washington, DC: US Environmental Protection Agency, Office of Modeling, Monitoring Systems, and Quality Assurance, Office of Ecological i.e. Environmental Processes and Effects Research, Office of Research and Development.
- Boltovskoy E and Totah V (1992) Preservation index and preservation potential of some foraminiferal species. *The Journal of Foraminiferal Research* 22(3): 267–273.
- Braden A, Lopez R and Silvy N (2005) *Effectiveness of Fencing, Underpasses, and Deer Guards in Reducing Key Deer Mortality on the US 1 Corridor, Big Pine Key, Florida*. College Station, TX: Department of Wildlife and Fisheries, Texas A & M University.
- Bregy JC, Wallace DJ, Minzoni RT, et al. (2018) 2500-year paleotempestological record of intense storms for the northern Gulf of Mexico, United States. *Marine Geology* 396: 26–42.
- Cangialosi JP, Latto AS and Berg R (2018) National Hurricane Center Tropical Cyclone Reports: Hurricane Irma. National Oceanic and Atmospheric Administration. Available from: https://www.nhc.noaa.gov/data/tcr/AL112017_Irma.pdf (accessed 7 April 2021).
- Carnahan EA, Hoare A, Hallock P, et al. (2009) Foraminiferal assemblages in Biscayne Bay, Florida, USA: Responses to urban and agricultural influence in a subtropical estuary. *Marine Pollution Bulletin* 59(8-12): 221–233.
- Chagué-Goff C, Nichol S, Jenkinson A, et al. (2000) Signatures of natural catastrophic events and anthropogenic impact in an estuarine environment, New Zealand. *Marine Geology* 167(3-4): 285–301.
- Chough SK (2012) *Geology and Sedimentology of the Korean Peninsula*. Amsterdam: Elsevier.
- Clarke KR, Gorley R, Somerfield PJ, et al. (2014) *Change in Marine Communities: An Approach to Statistical Analysis and Interpretation*. Plymouth: PRIMER-E Limited.
- Culver SJ (1990) Benthic foraminifera of Puerto Rican mangrove-lagoon systems; potential for paleoenvironmental interpretations. *Palaios* 5(1): 34–51.
- Donnelly JP and Woodruff JD (2007) Intense hurricane activity over the past 5,000 years controlled by El Niño and the West African monsoon. *Nature* 447(7143): 465–468.
- Ehrenhauss S, Witte U, Janssen F, et al. (2004) Decomposition of diatoms and nutrient dynamics in permeable North Sea sediments. *Continental Shelf Research* 24(6): 721–737.
- Felder DL and Camp DK (2009) *Gulf of Mexico Origin, Waters, and Biota: Biodiversity*. College Station, TX: Texas A&M University Press.
- González-Regalado M, Gómez P, Ruiz F, et al. (2019) Facies analysis, foraminiferal record and chronostratigraphy of Holocene sequences from Saltés Island (Tinto-Odiel estuary, SW Spain): the origin of high-energy deposits. *Estuarine, Coastal and Shelf Science* 218: 95–105.
- Gregory BR, Peros M, Reinhardt EG, et al. (2015) Middle-late Holocene Caribbean aridity inferred from foraminifera and elemental data in sediment cores from two Cuban lagoons. *Palaeogeography, Palaeoclimatology, Palaeoecology* 426: 229–241.
- Gregory BR, Reinhardt EG and Gifford JA (2017) The influence of morphology on sinkhole sedimentation at Little Salt Spring, Florida. *Journal of Coastal Research* 33(2): 359–371.
- Hallock P, Lidz BH, Cockey-Burkhard EM, et al. (2003) Foraminifera as bioindicators in coral reef assessment and monitoring: The FORAM index. *Environmental Monitoring and Assessment* 81(1): 221–238.

- Hammer Ø (2012) PAST PAleontological STatistics Version 2.17 Reference Manual. Natural History Museum, University of Oslo, 229.
- Hanson CE (1980) *Freshwater resources of Big Pine Key, Florida*. Reston, Virginia: U.S. Geological Survey.
- Harveson PM, Lopez RR, Silvy NJ, et al. (2004) Source-sink dynamics of Florida Key deer on Big Pine Key, Florida. *The Journal of Wildlife Management* 68(4): 909–915.
- Haslett S, Bryant EA and Curr R (2000) *Tracing Beach Sand Provenance and Transport Using Foraminifera: Preliminary Examples from Northwest Europe and Southeast Australia*. Hoboken, New Jersey: Wiley.
- Hawkes AD and Horton B (2012) Sedimentary record of storm deposits from Hurricane Ike, Galveston and San Luis Islands, Texas. *Geomorphology* 171: 180–189.
- Heiri O, Lotter AF and Lemcke G (2001) Loss on ignition as a method for estimating organic and carbonate content in sediments: Reproducibility and comparability of results. *Journal of Paleolimnology* 25(1): 101–110.
- Hippensteel SP and Martin RE (1999) Foraminifera as an indicator of overwash deposits, barrier island sediment supply, and barrier island evolution: Folly Island, South Carolina. *Palaeogeography, Palaeoclimatology, Palaeoecology* 149(1-4): 115–125.
- Hippensteel SP, Eastin MD and Garcia WJ (2013) The geological legacy of Hurricane Irene: Implications for the fidelity of the paleo-storm record. *GSA Today* 23(12): 4–10.
- Hippensteel SP, Martin RE and Harris MS (2005) Records of prehistoric hurricanes on the South Carolina coast based on micropaleontological and sedimentological evidence, with comparison to other Atlantic Coast records: Discussion. *Geological Society of America Bulletin* 117(1-2): 250–253.
- Holmes CW (2001) Short-lived isotopes in sediments (a tool for assessing sedimentary dynamics). *USGS Open File Report*. Reston, VA: US Geological Survey.
- Horton BP, Rossi V and Hawkes AD (2009) The sedimentary record of the 2005 hurricane season from the Mississippi and Alabama coastlines. *Quaternary International* 195(1-2): 15–30.
- Hottinger L (1997) Shallow benthic foraminiferal assemblages as signals for depth of their deposition and their limitations. *Bulletin de la Société géologique de France* 168(4): 491–505.
- Ishman SE, Graham I and D'Ambrosio J (1997) *Modern Benthic Foraminifer Distributions in Biscayne Bay: Analogs for Historical Reconstructions*. US Department of the Interior, US Geological Survey.
- Jiménez-Berrococo Á, Zuluaga MC and Elorza J (2004) Minor-and trace-element intra-shell variations in Santonian inoceramids (Basque-Cantabrian Basin, northern Spain): diagenetic and primary causes. *Facies* 50(1): 35–60.
- Kitto ME (1991) Determination of photon self-absorption corrections for soil samples. *International Journal of Radiation Applications and Instrumentation. Part A. Applied Radiation and Isotopes* 42(9): 835–839.
- Lane P, Donnelly JP, Woodruff JD, et al. (2011) A decadal-resolved paleohurricane record archived in the late Holocene sediments of a Florida sinkhole. *Marine Geology* 287(1-4): 14–30.
- Langevin C, Stewart MT and Beaudoin C (1998) Effects of sea water canals on fresh water resources: an example from Big Pine Key, Florida. *Groundwater* 36(3): 503–513.
- Liu K-b and Fearn ML (2000) Reconstruction of prehistoric landfall frequencies of catastrophic hurricanes in northwestern Florida from lake sediment records. *Quaternary Research* 54(2): 238–245.
- Liu K-b, McCloskey TA, Blanchette TA, et al. (2014) Hurricane Isaac storm surge deposition in a coastal wetland along Lake Pontchartrain, southern Louisiana. *Journal of Coastal Research* (70): 266–271.
- Loeblich JRA and Tappan H (1987) *Foraminiferal Genera and their Classification*. New York: Van Reinhold Company, 2.
- Möller I, Kudella M, Rupprecht F, et al. (2014) Wave attenuation over coastal salt marshes under storm surge conditions. *Nature Geoscience* 7(10): 727–731.
- Murray JW (2014) *Ecology and Palaeoecology of Benthic Foraminifera*. Routledge.
- Nelson DW and Sommers LE (1996) Total carbon, organic carbon, and organic matter. In: Sparks DL, Page AL, Helmke PA, et al (eds) *Methods of Soil Analysis: Part 3 Chemical Methods*, 5.3. Madison, WI: American Society of Agronomy, Crop Science Society of America, and Soil Science Society of America, pp. 961–1010.
- Ogurcak DE and Price RM (2019) Groundwater geochemistry fluctuations along a fresh-saltwater gradient on the carbonate islands of the lower Florida Keys. *Chemical Geology* 527: 118925.
- Oliva F, Peros M and Viau A (2017) A review of the spatial distribution of and analytical techniques used in paleo-tempestological studies in the western North Atlantic Basin. *Progress in Physical Geography* 41(2): 171–190.

- Oliva F, Viau AE, Peros MC, et al. (2018) Paleotemperature database for the western North Atlantic basin. *The Holocene* 28(10): 1664–1671.
- Olsson IU (1986) *Radiometric Dating. Handbook of Holocene Palaeoecology and Palaeohydrology*. Chichester, UK: John Wiley and Sons.
- Orbigny A (1839) *Foraminifères*. A. Bertrand.
- Patricola CM and Wehner MF (2018) Anthropogenic influences on major tropical cyclone events. *Nature* 563(7731): 339–346.
- Pilarczyk JE, Dura T, Horton BP, et al. (2014) Microfossils from coastal environments as indicators of paleo-earthquakes, tsunamis and storms. *Palaeogeography, Palaeoclimatology, Palaeoecology* 413: 144–157.
- Pilarczyk JE, Horton BP, Witter RC, et al. (2012) Sedimentary and foraminiferal evidence of the 2011 Tōhoku-oki tsunami on the Sendai coastal plain, Japan. *Sedimentary Geology* 282: 78–89.
- Ramírez-Herrera M-T, Lagos M, Hutchinson I, et al. (2012) Extreme wave deposits on the Pacific coast of Mexico: Tsunamis or storms?—A multi-proxy approach. *Geomorphology* 139: 360–371.
- Riou B, Chaumillon E, Chagué C, et al. (2020) Backwash sediment record of the 2009 South Pacific Tsunami and 1960 Great Chilean Earthquake Tsunami. *Scientific Reports* 10(1): 1–13.
- Saha S, Bradley K, Ross MS, et al. (2011) Hurricane effects on subtropical pine rocklands of the Florida Keys. *Climatic Change* 107(1): 169–184.
- Savrda CE, Bottjer DJ and Gorsline DS (1984) Development of a comprehensive oxygen-deficient marine biofacies model: evidence from Santa Monica, San Pedro, and Santa Barbara Basins, California Continental Borderland. *AAPG Bulletin* 68(9): 1179–1192.
- Schwing PT, Romero IC, Larson RA, et al. (2016) Sediment core extrusion method at millimeter resolution using a calibrated, threaded-rod. *Journal of Visualized Experiments* 114: 54363.
- Scott DB, Collins E, Gayes P, et al. (2003) Records of prehistoric hurricanes on the South Carolina coast based on micropaleontological and sedimentological evidence, with comparison to other Atlantic Coast records. *Geological Society of America Bulletin* 115(9): 1027–1039.
- Sen Gupta B (ed) (1999) *Modern Foraminifera*. Dordrecht: Kluwer academic Publishers.
- Shao W, Xian S, Keim BD, et al. (2017) Understanding perceptions of changing hurricane strength along the US Gulf coast. *International Journal of Climatology* 37(4): 1716–1727.
- Shepard CC, Crain CM and Beck MW (2011) The protective role of coastal marshes: A systematic review and meta-analysis. *PloS One* 6(11): e27374.
- Snaiki R, Wu T, Whittaker AS, et al. (2020) Hurricane wind and storm surge effects on coastal bridges under a changing climate. *Transportation Research Record* 2674(6): 23–32.
- Sturdivant SK, Díaz RJ and Cutter GR (2012) Bioturbation in a declining oxygen environment, in situ observations from Wormcam. *PloS One* 7(4): e34539.
- Sun Loh P, Molot LA, Nowak E, et al. (2013) Evaluating relationships between sediment chemistry and anoxic phosphorus and iron release across three different water bodies. *Inland Waters* 3(1): 105–118.
- Swindles GT, Galloway JM, Macumber AL, et al. (2018) Sedimentary records of coastal storm surges: Evidence of the 1953 North Sea event. *Marine Geology* 403: 262–270.
- Tanaka H, Tinh NX, Umeda M, et al. (2012) Coastal and estuarine morphology changes induced by the 2011 Great East Japan Earthquake Tsunami. *Coastal Engineering Journal* 54(01): 1250010.
- US Geological Survey (2017) USGS measures the impacts of Hurricane Irma. Available from: <https://www.usgs.gov/news/usgs-measures-impacts-hurricane-irma> (accessed 12 December 2017).
- Vacher LH and Quinn TM (2004) *Geology and Hydrogeology of Carbonate Islands*. Elsevier.
- Villanova VL, Hughes PT and Hoffman EA (2017) Combining genetic structure and demographic analyses to estimate persistence in endangered Key deer (*Odocoileus virginianus clavium*). *Conservation Genetics* 18(5): 1061–1076.
- Wang P and Chappell J (2001) Foraminifera as Holocene environmental indicators in the South Alligator River, northern Australia. *Quaternary International* 83: 47–62.
- Webster PJ, Holland GJ, Curry JA, et al. (2005) Changes in tropical cyclone number, duration, and intensity in a warming environment. *Science* 309(5742): 1844–1846.
- Weinkle J, Landsea C, Collins D, et al. (2018) Normalized hurricane damage in the continental United States 1900–2017. *Nature Sustainability* 1(12): 808–813.
- Wilson B (2006) The environmental significance of *Archaias angulatus* (Miliolida, Foraminifera) in sediments around Nevis, West Indies. *Caribbean Journal of Science* 42(1): 20.

- Yao Q, Liu K-b and Ryu J (2018) Multi-proxy characterization of Hurricanes Rita and Ike storm deposits in the Rockefeller Wildlife Refuge, southwestern Louisiana. *Journal of Coastal Research* (85): 841–845.
- Yao Q, Liu K-B, Williams H, et al. (2020) Hurricane Harvey storm sedimentation in the San Bernard national wildlife refuge, Texas: Fluvial versus storm surge deposition. *Estuaries and Coasts* 43(5): 971–983.